Supplemental material: Many-body subradiant excitations in metamaterial arrays: Experiment and theory

Stewart D. Jenkins and Janne Ruostekoski
Mathematical Sciences and Centre for Photonic Metamaterials, University of Southampton, Southampton SO17 1BJ, United Kingdom

Nikitas Papasimakis[1], Salvatore Savo[1,2], and Nikolay I. Zheludev[1,3]
[1] *Optoelectronics Research Centre and Centre for Photonic Metamaterials, University of Southampton Southampton SO17 1BJ, United Kingdom*
[2] *TetraScience Inc., 114 Western Ave, Boston, MA, 02134*
[3] *Centre for Disruptive Photonic Technologies, School of Physical and Mathematical Sciences and The Photonics Institute, Nanyang Technological University, Singapore 637378, Singapore*
(Dated: June 20, 2017)

Here we provide a detailed description of the theoretical formalism and the numerical modelling, and present additional figures of the eigenmode contributions of the steady-state spectral response. We also provide details on the microwave samples and experimental setup.

Numerical model

Radiative coupling between the resonators

We briefly describe the numerical simulations of the electromagnetic (EM) response of a planar metamaterial array. The general formalism to describe interacting magnetodielectric resonators is presented in [1]. For the rectangular array of asymmetric split ring (ASR) metamolecules we represent each meta-atom j by a single mode of current oscillation that behaves as an effective RLC circuit with resonance frequency ω_j. We label the meta-atoms by indices j ($j = 1, \ldots, 2N$) such that the ℓth ASR metamolecule includes the two meta-atoms $2\ell - 1$ and 2ℓ. In a symmetric split ring (SSR) metamolecule the resonance frequencies of the two meta-atoms are equal ω_0, but in the ASRs the symmetry is broken by adjusting the lengths of the resonators in such a way that the resonance frequencies of the two arcs in each ASR metamolecule become $\omega_0 \pm \delta\omega$.

In the following discussion for the radiative interactions between the resonators, all the field and resonator amplitudes refer to the slowly-varying versions of the positive frequency components of the corresponding variables, where the rapid oscillations $e^{-i\Omega t}$ ($k = \Omega/c$) due to the frequency, Ω, of the incident wave have been factored out in the rotating wave approximation. The current excitations in the meta-atoms interact with the propagating field and radiate electric and magnetic fields. Each meta-atom is treated in the point dipole approximation with an electric dipole $\mathbf{d}_j(t) = d_j(t)\hat{\mathbf{e}}_y$ and magnetic dipole $\mathbf{m}_j(t) = m_j(t)\hat{\mathbf{m}}_j$, where $\hat{\mathbf{m}}_{2\ell} = -\hat{\mathbf{m}}_{2\ell-1} \equiv \hat{\mathbf{m}} = \hat{\mathbf{e}}_z$; see Fig. 1 in the main section. The normal mode amplitude of the current excitations in the meta-atom j then reads [1]

$$b_j(t) = \left(\frac{k^3}{12\pi\epsilon_0}\right)^{1/2}\left(\frac{d_j(t)}{\sqrt{\Gamma_\mathrm{e}}} + i\frac{m_j(t)}{c\sqrt{\Gamma_\mathrm{m}}}\right). \tag{1}$$

Here Γ_e and Γ_m denote the electric and magnetic dipole decay rates of an isolated meta-atom, respectively. The total decay rate of the meta-atom excitations is then $\Gamma = \Gamma_\mathrm{e} + \Gamma_\mathrm{m} + \Gamma_\mathrm{o}$, where we have also added a nonradiative loss rate Γ_o.

Moreover, the scattered fields are given by $\mathbf{E}_S = \sum_j \mathbf{E}_S^{(j)}$ and $\mathbf{H}_S = \sum_j \mathbf{H}_S^{(j)}$ where the contributions from the meta-atom j read

$$\mathbf{E}_S^{(j)}(\mathbf{r},t) = \frac{k^3}{4\pi\epsilon_0}\left[\mathsf{G}(\mathbf{r}-\mathbf{r}_j)\mathbf{d}_j + \frac{1}{c}\mathsf{G}_\times(\mathbf{r}-\mathbf{r}_j)\mathbf{m}_j\right], \tag{2}$$

$$\mathbf{H}_S^{(j)}(\mathbf{r},t) = \frac{k^3}{4\pi}\left[\mathsf{G}(\mathbf{r}-\mathbf{r}_j)\mathbf{m}_j - c\mathsf{G}_\times(\mathbf{r}-\mathbf{r}_j)\mathbf{d}_j\right]. \tag{3}$$

The radiation kernel $\mathsf{G}(\mathbf{r}-\mathbf{r}_j)$ determines the electric (magnetic) field at $\mathbf{r}$, from an oscillating electric (magnetic) dipole of the meta-atom j at $\mathbf{r}_j$ [2]. The cross kernel $\mathbf{G}_\times(\mathbf{r}-\mathbf{r}_j)$ describes the electric (magnetic) field at $\mathbf{r}$ an oscillating magnetic (electric) dipole at $\mathbf{r}_j$.

Each meta-atom is driven by the incident fields, $\boldsymbol{\mathcal{E}}_0(\mathbf{r},t)$ and $\boldsymbol{\mathcal{H}}_0(\mathbf{r},t)$, and the fields scattered by all the other resonators in the system,

$$\mathbf{E}_\mathrm{ext}(\mathbf{r}_j,t) = \boldsymbol{\mathcal{E}}_0(\mathbf{r},t) + \sum_{l\neq j}\mathbf{E}_S^{(l)}(\mathbf{r},t), \tag{4}$$

$$\mathbf{H}_\mathrm{ext}(\mathbf{r}_j,t) = \boldsymbol{\mathcal{H}}_0(\mathbf{r},t) + \sum_{l\neq j}\mathbf{H}_S^{(l)}(\mathbf{r},t)\,, \tag{5}$$

where the scattered fields are given by Eqs. (2) and (3). The EM fields couple to the current excitations of the meta-atom via its electric and magnetic dipole moments according to Eq. (1).

Collecting these together, we obtain a coupled set of equations between the meta-atom excitations that describe the EM field mediated interactions. In terms of $\mathrm{b} \equiv (b_1, b_2, \ldots, b_{2N})^T$, we may write them as [1]

$$\dot{\mathrm{b}} = \mathcal{C}\mathrm{b} + \mathrm{F}(t)\,. \tag{6}$$

The off-diagonal elements of the matrix $\mathcal{C}$ describe radiative interactions between the different arcs mediated by the scattered field that incorporate the retardation effects with short- and long-range interactions. The diagonal elements represent the damped free oscillations of the arcs. The driving of the meta-atom by the incident field is encapsulated in $\mathrm{F}(t)$. Evaluating the normal mode excitations of the system and the corresponding scattered fields (2) and (3) then yield the metamaterial array's response.

Steady-state response

In the numerical simulations of the planar metamaterial illuminated by the driving fields, we solve the steady-state response,

$$\mathrm{b} = -\mathcal{C}^{-1}\mathrm{F}\,, \tag{7}$$

obtained from (6).

In our simulations we consider the experimental arrangement of the 30×36 array of ASR metamolecules, with the single metamolecule magnetic and electric decay rates satisfying $\Gamma_\mathrm{e} = \Gamma_\mathrm{m}$. In the microwave ASR system the nonradiative losses are almost solely due to the supporting substrate and we incorporate these in the numerical model by setting $\Gamma_\mathrm{o} = 0.07\Gamma$. For the plasmonic system the nonradiative loss rate $\Gamma_\mathrm{o} = 0.25\Gamma$ is chosen to be comparable with those observed for Fano resonance experiments on gold rods [3] and obtained by Drude-model based estimates [4].

For the microwave (plasmonic) case we consider a lattice spacing $a = 0.28\lambda$ ($a = 0.2\lambda$), the separation of the two meta-atoms in each metamolecule 0.114λ (0.075λ), and the asymmetry between the two arcs of a metamolecule $\delta\omega = 0.3\Gamma$ ($\delta\omega = 0.7\Gamma$).

In order to model the effects of the nonuniform illumination in the response of the array, we input the experimentally measured incident field profile in the numerical calculations.

Eigenmode calculations

In a metamaterial array, we have a system of N ASR meta-molecules, or $2N$ single-mode resonators (meta-atoms). These possess $2N$ collective modes of current oscillation, with corresponding collective resonance frequencies and decay rates. We calculate the eigenmodes of the entire 30×36 planar metamaterial system of 2160 interacting meta-atoms by diagonalizing the matrix $\mathcal{C}$. In Fig. 3(b) of the main section we also calculate the eigenmodes by varying the size of the array. We generally consider the two cases with the array consisting of (i) SSR metamolecules and (ii) ASR metamolecules. The description of the response in terms of the eigenmodes of the SSR array (i) is useful in explaining the emergent Fano resonance when the system becomes more strongly interacting. Specifically, the Fano resonance results from the destructive interference between the phase-coherent electric (PE) and phase-coherent magnetic (PM) dipole modes. Diagonalizing the system (ii), on the other hand, provides the true eigenmodes of the system and shows how the steady-state excitation of the array is dominated by the spatially extended multimetamolecule subradiant mode.

Subradiant modes and the relationship to other physical systems

The PE and PM modes represents excitations where the metamolecules oscillate in phase; in the PE mode the two arcs are symmetrically excited (the currents in the two arcs oscillate in phase) and in the PM mode the two arcs are antisymmetrically excited (the current oscillate π out of phase). We can extend the metamolecule analogy of molecular wavefunctions to the ASRs. In the symmetric (i) metamolecule case (SSR) the metamolecule eigenfunctions would be similar to the classical versions of the wavefunctions of a homonuclear dimer molecule. An entangled quantum state of the dimer molecule with precisely single excitation reads

$$|\Psi_\pm\rangle = \frac{1}{\sqrt{2}}\left(|1,g;2,e\rangle \pm |1,e;2,g\rangle\right)\,, \tag{8}$$

where g and e denote the ground and excited states, respectively, and 1 and 2 are the two atoms of the dimer. Since the excited state has an odd symmetry, $|\Psi_-\rangle$ has an even symmetry and $|\Psi_+\rangle$ odd. Then the subradiant gerade $|\Psi_-\rangle$ corresponds to the antisymmetric mode of the metamolecule ℓ, $(\ell,-)$, and the superradiant ungerade $|\Psi_+\rangle$ to the symmetric mode of the metamolecule ℓ, $(\ell,+)$.

The circuit resonators are assumed to respond linearly to the EM fields. Two-level systems, such as atoms, experience an analogous response to light as classical harmonic oscillators in the low light intensity limit when driven by a coherent field amplitude [5, 6]. A single photon excitation (8) exhibits quantum entanglement and can display quantum statistics in the properties of the emitted light – a limit that would be challenging to reach in the studied circuit resonator system with notable thermal excitations and a linear response. However, as a single excitation in an ensemble of two-level emitters

does not experience saturation, its excitation dynamics in terms of the Schrödinger amplitudes is identical to that of the coupled driven classical oscillators [7]. This illustrates how our subradiance system shares similar properties to correlated subradiant excitations in other physical systems when they are driven in the classical limit, and even when the excitations are quantum mechanical. In fact, analogous numerical simulation techniques that we are using here can also be derived for the studies of the interactions of light with ensembles of cold atoms [8], and atoms confined in periodic arrays can be reminiscent of the planar metamaterial systems [9]. The differences from the circuit resonators are mostly notable if collective excitations studied in the atomic systems with multiple electronic levels [10] or in nonlinearly responding quantum systems [11]. It is also interesting to point out that for atoms the spontaneous emission rate results from vacuum fluctuations and here the corresponding decay rates can also be derived from first principles [1], but the origin of the decay rates is now entirely classical, resulting from the self-interaction of the polarization density with its own scattered radiation.

Distribution of decay rates

In the main text the emphasis is on the superradiant and subradiant modes that participate most strongly in the response. However, among the rest of the modes there are also eigenmodes with notably narrower linewidths. For example, for the SSR system the eigenmodes exhibit a broad distribution of resonance frequencies and decay rates. We find that the largest decay rate in the system, corresponding to the most superradiant mode, is about 14.5Γ. The smallest decay rate is negligibly small compared with nonradiative losses with the value of $9.4 \times 10^{-10}\Gamma$. Due to extremely weak coupling of this mode to external fields, its excitation is very challenging.

Eigenmode contributions of the excitations

The different eigenmode contributions of the steady-state excitations were shown in the main section of the paper, where PM and PE modes were shown to characterize the Fano transmission resonance. In Fig. 1 we compare the occupations of the steady-state excitation in the two eigenmode basis, one formed by the interacting SSR metamolecules and the other one by the interacting ASR metamolecules. The SSR one is the same as Fig. 3(a) in the main section. The ASR curves illustrate the overwhelmingly dominant excitation of the subradiant eigenmode of the ASR array. In Fig. 2, we present the corresponding occupations for plasmonic metamaterial arrays. Similarly to the microwave case, the subradiant eigenmode dominates over the coherent electric dipole mode, although other modes provide also provide strong contributions.

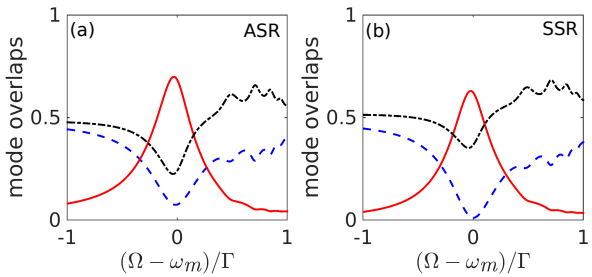

FIG. 1. Contributions of dominantly electric (solid red line) and magnetic (dashed blue line) eigenmodes to the steady-state excitation of microwave ASR arrays under a decomposition in ASR (a) and SSR (b) eigenmodes. The sum of the contributions of all the other modes is marked by a dashed-dotted black line in both panels.

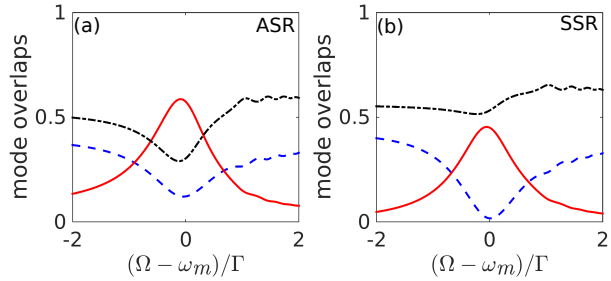

FIG. 2. Contributions of dominantly electric (solid red line) and magnetic (dashed blue line) eigenmodes to the steady-state excitation of plasmonic ASR arrays under a decomposition in ASR (a) and SSR (b) eigenmodes. The sum of the contributions of all the other modes is marked by a dashed-dotted black line in both panels.

Experimental setup and samples

Asymmetrically-split ring (ASR) metamaterial arrays were manufactured by etching a 35 μm copper cladding on an FR4 printed circuit board (PCB) substrate. The thickness of the substrate is 1.6 mm, whereas its permittivity is $\epsilon \simeq 4.5 + 0.15i$. Each ASR has an inner and outer radius of 2.8 and 3.2 mm, respectively, with $\Gamma = 3.5$ GHz. The asymmetry is introduced by a difference in length of the two arcs, corresponding to angles 160° and 140°. The array consists of 30×36 unit cells, each with dimensions of $7.5 \times 7,5$ mm^2.

Transmission and reflectivity measurements were performed in an anechoic chamber with broadband linearly polarized antennas (Schwarzbeck BBHA 9120D) at normal incidence, where the electric field amplitude and phase was recorded by a vector network analyzer (Agilent

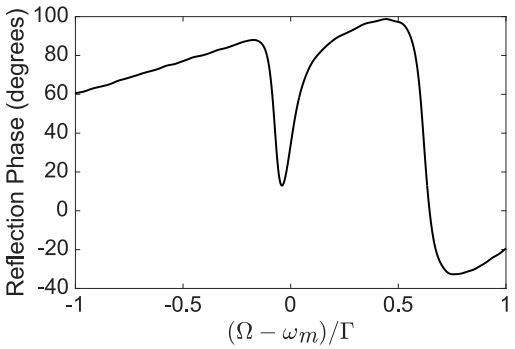

FIG. 3. Experimentally measured reflection phase spectrum from an ASR array. The corresponding reflectance is presented in Fig. 2a in the main text.

E8364B) in the range of $2 - 18$ GHz. The polarization of the incident wave was normal to the plane of symmetry of the ASR. Near-field mapping of the metamaterial sample was performed in a microwave scanning-near field microscope, where an electric monopole with a length of 2.5 mm was mounted on a motorized stage and collected the near electric field at a distance of 1 mm from the metamaterial. The spatial resolution in the sample plane was 1 mm.

We woud like to note here that the microwave measurements allow to record both amplitude and phase, hence providing all information required to fully characterize the response of the metamaterials. A typical example of a phase trace is presented in Fig. S3, which corresponds to the experimental reflectivity spectrum of Fig. 2a in the main text.

[1] S. D. Jenkins and J. Ruostekoski, Phys. Rev. B **86**, 085116 (2012).

[2] J. D. Jackson, *Classical Electrodynamics*, 3rd ed. (Wiley, New York, 1999).

[3] N. Liu, L. Langguth, T. Weiss, J. Kästel, M. Fleischhauer, T. Pfau, and H. Giessen, Nat. Mater. **8**, 758 (2009).

[4] H. Kuwata, H. Tamaru, K. Esumi, and K. Miyano, Applied Physics Letters **83**, 4625 (2003).

[5] J. Ruostekoski and J. Javanainen, Phys. Rev. A **55**, 513 (1997).

[6] M. D. Lee, S. D. Jenkins, and J. Ruostekoski, Phys. Rev. A **93**, 063803 (2016).

[7] A. A. Svidzinsky, J.-T. Chang, and M. O. Scully, Phys. Rev. A **81**, 053821 (2010).

[8] J. Javanainen, J. Ruostekoski, B. Vestergaard, and M. R. Francis, Phys. Rev. A **59**, 649 (1999).

[9] S. D. Jenkins and J. Ruostekoski, Phys. Rev. A **86**, 031602(R) (2012).

[10] M. Hebenstreit, B. Kraus, L. Ostermann, and H. Ritsch, Phys. Rev. Lett. **118**, 143602 (2017).

[11] F. Nissen, J. M. Fink, J. A. Mlynek, A. Wallraff, and J. Keeling, Phys. Rev. Lett. **110**, 203602 (2013).